공학석사 학위논문

Highly sensitive and selective visual detection of Cr(VI) ions based on etching of silver-coated gold nanorods

은이 코팅된 금 나노막대가 에칭 되는 현상을 기반으로 한 6가 크롬 검출 색 센서

2017년 2월

서울대학교 융합과학기술대학원

융합과학부 나노융합전공

김 다 솜

Highly sensitive and selective visual detection of Cr(VI) ions based on etching of silver-coated gold nanorods

지도 교수 박 원 철

이 논문을 공학석사 학위논문으로 제출함

2017년 02월

서울대학교 융합과학기술대학원

융합과학부 나노융합전공

김 다 솜

김다솜의 석사학위논문을 인준함

2016 년 12 월

위 원 장 김 연 상 (인)

부위원장 박 원 철 (인)

위 원 송 윤 규 (인)

Highly sensitive and selective visual detection of Cr(VI) ions based on etching of silver-coated gold nanorods

Dasom Kim

Program in Nano Science and Technology

Graduate School of Convergence Science & Technology

Seoul National University

Abstract

We report a simple and cost-effective visual detection of Cr(VI) ions using silver-coated gold nanorods (AuNR@Ag) as sensing probes. Au nanorods (Au NRs) were prepared by a seed-mediated growth process and AuNR@Ag nanostructures were synthesized by growing Ag nanoshells on Au NRs. Successful coating of Ag nanoshells on the surface of Au NRs was demonstrated with TEM, EDS, and UV-vis spectrometer. By increasing the overall amount of the deposited Ag on Au NRs, the localized surface plasmon resonance (LSPR) band was significantly blue-shifted, which allowed tuning across the visible spectrum. The sensing mechanism relies on the redox reaction between Cr(VI) ions and Ag nanoshells on Au NRs. As the concentration of Cr(VI) ions increased, more significant red-shift of the longitudinal peak and intensity decrease of the transverse peak could be observed using UV-vis spectrometer. Several parameters such as concentration of CTAB, thickness of the Ag nanoshells and pH of the sample were carefully optimized to

determine Cr(VI) ions. Under optimized condition, this method showed a low detection limit of 20 nM and high selectivity towards Cr(VI) ion over other metal ions, and the detection range of Cr(VI) ion was tuned by controlling thickness of the Ag nanoshells. From multiple evaluations in real sample, it is clear that this method is a promising Cr(VI) ion colorimetric sensor with rapid, sensitive, and selective sensing ability.

Keywords: Gold nanorod, Silver nanoshell, Cr(VI) ion, Etching, Colorimetric sensor

Student Number: 2015-26023

Contents

List of Figures

Figure 12 Selectivity of the AuNR@Ag3 sensing system. (A) Photographic images and (B) the UV-vis spectra of AuNR@Ag3 based detection systems with various metal ions. (The concentration of Ag^{+}, Ca^{2+}, Zn^{2+}, Cd^{2+}, Al^{3+}, Ba^{2+}, Co^{2+}, Hg^{2+}, Fe^{2+}, Mn^{2+}, K^{+}, Na^{+}, Li^{+}, Mg^{2+}, Ni^{+}, or Pb^{2+} was 1×10^{-4} M and the concentration of Cr(VI) was 1×10^{-6} M)

List of Tables

1. Introduction

1.1 Cr(III) and Cr(VI)

Cr(III) and Cr(VI) are two main modes of chromium occurrence in aqueous solutions and Cr(III) is one of the essential trace elements in metabolism of glucose and lipids in human body.[1] Cr(III) deficiency may lead to increased cholesterol and blood lipids.[2, 3] Some Cr(III) compounds such as Cr(III) picolinate have been employed as supplemental or alternative medication for diabetes.[4] However, Cr(VI) is well known for its extremely carcinogenic and mutagenic effects and is one of the most critical environmental pollutants.[5, 6] Thus, the U.S. Environmental Protection Agency (EPA) recommends a Cr(VI) concentration of 1 μM (50 ppb) in drinking water as "maximum contaminant level goals".[7] Cr(VI) has been widely used in many industrial processes including chrome plating, textile industries, leather tanning, and wood preserving. Due to the increasing threat of Cr(VI) exposure in the environment, much more attention has been attracted to highly sensitive and selective assays for the determination of Cr(VI).[8] A multitude of detection methods for chromium have been reported before and most of these systems include inductively coupled plasma mass spectrometry (ICP-

MS),[9] atomic absorption spectrometry(AAS),[10] inductively coupled plasma atomic emission spectrometry(ICP-AES)[11] and electrochemical methods.[12, 13] Although these methods have high sensitivity and excellent selectivity, they usually require expensive instruments and skilled personnel. Additionally, these methods are not suitable for on-site analysis or in resource-poor settings. Visual methods can be convenient and attractive in many applications because they can be easily observed with the naked eyes without the aid of any advanced instruments.[14, 15]

1.2 Optical Properties of Nanomaterials

With advances in nanotechnology, noble metal nanomaterials have been widely studied for various applications such as chemical and biochemical sensing.[16-20] In recent years, the interest in Ag and Au nanoparticles(NPs) has dramatically increased, mostly due to their unique optical response which is often called as localized surface plasmon resonance (LSPR).[21, 22] The LSPR is a specific type of plasma oscillation occurring at lower energies than bulk plasmon, which happens when light is coupled to the coherent oscillation of free electrons at the surface of a conductor.

When the particle dimensions are too small to support a propagating wave, light will interact with metal particles smaller than the wavelength of incident light to generate a LSPR.[23] The LSPR of Au and Ag NPs is highly dependent on their size, shape, surface charge and local dielectric environment.[24] As illustrated in Figure 1, spherical NPs have a single, sharp absorption band due to the excitation of what is called a dipole plasmon resonance, where the entire charge distribution of the particle oscillates at the frequency of the incident electric field. For Au NPs, the resonance condition is satisfied at visible wavelengths, which attributing for its intense color. Au NP colloid solutions in the 10 nm size range have a strong absorption peak around 520 nm due to their LSPR. [35, 36] Anisotropic NPs show unique optical properties different from spherical NPs. For example, Au NRs possess two principal plasmon absorption bands: a transverse LSPR band and a longitudinal LSPR band. The two band positions depend on both the aspect ratio and the absolute dimensions of the particles (Figure 2).[25-27] Therefore, anisotropic NPs and spherical NPs with unique shape-dependent properties can be extensively explored as colorimetric probes for the detection of ions, small molecules, DNA and protein. [28-34]

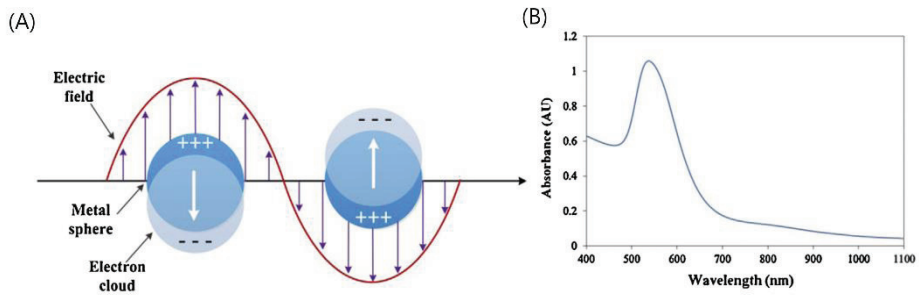

Figure 1 (A) Schematic diagram illustrating of LSPR for Au NPs.(From Ref. [35], K.A. Willets, R.P.V. Duyne, *Annu. Rev. Phys. Chem.* 58(1) (2007) 267-297.) (B) A typical LSPR absorption band of Au NPs. (From Ref. [36], J. Cao, T. Sun, K.T.V. Grattan, *Sensors Actuat. B-Chem.* 195 (2014) 332-351.)

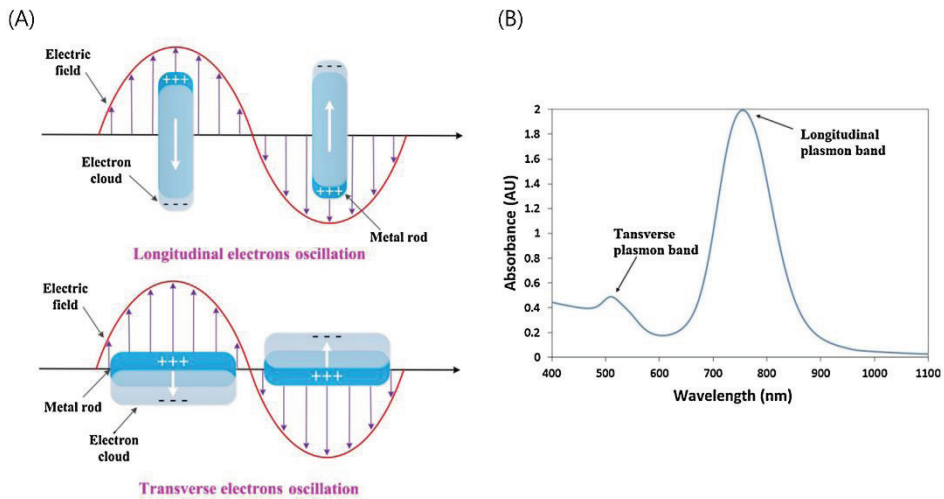

Figure 2 (A) Schematic diagrams illustrating of LSPR for Au NRs and (B) Two principal plasmon absorption bands: a transverse LSPR band and a longitudinal LSPR band corresponding to the electron oscillation along the long axis (Figure 2 (A) top) and the short axis (Figure 2 (A) below) of Au NRs, respectively. (From Ref. [36], J. Cao, T. Sun, K.T.V. Grattan, *Sensors Actuat. B-Chem.* 195 (2014) 332-351.)

1.3 Colorimetric Sensing Strategies

Nanomaterial-based colorimetric methods are commonly based on the change of optical properties due to aggregations, morphology transition, accompany by distinct color change. Two key components are essentially necessary in a colorimetric assay and affect the performance in selectivity, sensitivity and response time. Based on the behavior of nanoparticles, colorimetric sensing strategies can be summarized as two types: one is based on the analyte-induced aggregation of nanoparticles, called aggregation based method. The other mainly uses the morphology transition, which is called non-aggregation based method. The aggregation of the noble metal nanoparticles of appropriate sizes induces interparticle surface plasmon coupling, result in a visible color change.[37] Taking advantage of these characteristics, lots of colorimetric sensors are based on the aggregation of these metal nanoparticles.[38-41] For example, Chen *et al.* developed an Au NP-based colorimetric assay for Cr(VI) ions detection using the coordinate covalent bond between *meso*-2,3-dimercaptosuccinic acid-Au NPs and Cr(VI) (Figure 3).[42] This sensor is accessible for on-site application through translation of the colorimetric signal into the digital signal using a smartphone but still requires procedures for the modification of nanoparticles.

Also, this sample cause auto-aggregation and affect the stability of the sensor. Ravindran *et al.* reported a method for the detection of Cr(VI) using Ag NPs based on the aggregation-induced color change.[43] Although this sensor was easily prepared by unmodified Ag NPs and high selectivity of this sensor has not been thoroughly verified. Recently, Alex *et al.* developed a non-aggregation based and highly selective Cr(VI) detection method by using etching reactions of Au NRs (Figure 4).[44] Compared with aggregation colorimetric sensors, these a non-aggregation based sensors use simple procedures and show improved linearity. Herein, we designed a novel morphology transition based sensor by using silver-coated gold nanorods (AuNR@Ag) as sensing probes for the determination of trace Cr(VI). Our sensing method was based on redox reaction between Cr(VI) ion and Ag nanoshells on the surface of AuNR@Ag. By monitoring the change in the color and the LSPR peak, we could be quantitatively determine the Cr(VI) concentration with good linearity. Compared with Au NRs, AuNR@Ag nanostructures produce a much stronger and sharper plasmon resonance, showing considerably superior sensitivity to Au NRs sensor. Under optimized condition, this sensor shows high selectivity towards Cr(VI) over other metal ions and detection limit as low as 20 nM. The detection range of Cr(VI) could be tuned by controlling thickness of the Ag nanoshells. Real samples were also tested to confirm the practicability and the

results proved that our sensor has good performance in terms of selectivity, sensitivity, linearity, and low limit of detection. This is due to the high extinction coefficient of AuNR@Ag and the signal amplification effect of Ag nanoshells [45-47]. The longitudinal plasmon resonance of AuNR@Ag was blue-shifted as the deposited Ag nanoshells becomes thicker, which could be lead to apparent multicolor change.

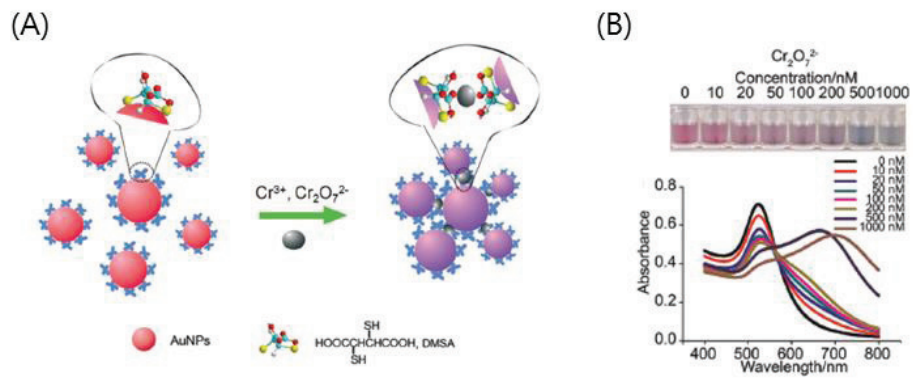

Figure 3 (A) Chromium ions induced colorimetric response of DMSA-Au NPs. (B) Photographs of and UV-Vis spectra of various concentrations of $Cr_2O_7^{2-}$ From 0 nM to 1000 nM in DMSA-Au NPs and the UV-Vis spectra of various concentrations of $Cr_2O_7^{2-}$ in DMSA-Au NPs. (From Ref. [43], W. Chen, F. Cao, W. Zheng, Y. Tian, Y. Xianyu, P. Xu, W. Zhang, Z. Wang, K. Deng, X. Jiang, *Nanoscale* 7(5) (2015) 2042-2049.)

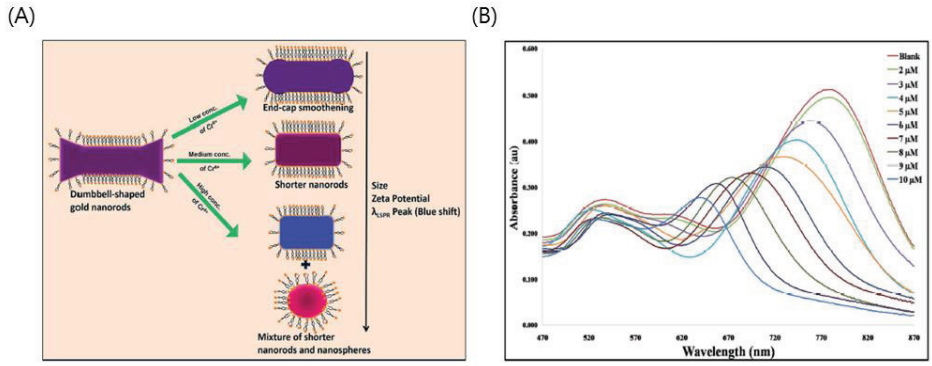

Figure 4 (A) Schmatic representation Cr(VI) concentration-dependent preferential etching. (B) UV-Vis spectra of Au NRs after the interaction with different concentrations of Cr(VI) (2-10 µM). (From Ref. [45], S.A. Alex, J. Satija, M.A. Khan, G.M. Bhalerao, S. Chakravarty, B. Kasilingam, A. Sivakumar, N. Chandrasekaran, A. Mukherjee, *Anal. Methods* 7(13) (2015) 5583-5592.)

2. Experimental section

2.1 Chemicals

Gold(III) chloride trihydrate ($HAuCl_4 \cdot 3H_2O$), cetyltrimethylammonium bromide (CTAB), silver nitrate ($AgNO_3$) and L-ascorbic acid (AA) were all obtained from Sigma-Aldrich. Sodium borohydride ($NaBH_4$) and sodium hydroxide (NaOH) were purchased from SAMCHUN chemical. CrO_3, $AgNO_3$, $Ca(CH_3COO)_2$, $Cd(CH_3COO)_2$, $AlCl_3$, $BaCl_2$, $CoCl_2$, $FeSO_4$, $MnCl_2$, NaOH, $Pb(CH_3COO)_2$, $LiCH_3COO$, $Mg[CH_3COCHC(O)CH_3]_2$ were bought from Sigma-Aldrich. $Hg(CH_3COO)_2$, $FeSO_4$, $ZnCl_2$, KCl, NaOH, $Ni(NO_3)_2$ were procured from SAMCHUN chemical. Ultrapure deionized water was used to prepare all solutions.

2.2 Apparatus

The Au NRs and AuNR@Ag were characterized by high-resolution (HR) transmission electron microscopy (TEM) using a JEOL JEM-2100F instrument, equipped with an energy-dispersive X-ray spectroscopy (EDX) detector. Ultraviolet visible (UV-vis) absorption spectra were collected on a Perkin Elmer Lambda 35 spectrometer. Inductively coupled plasma mass spectroscopic (ICP-MS)

measurements were performed with a Perkin Elmer SCIEX NEXION 350D instrument.

2.3 Preparation of Au NRs

Au NRs were synthesized according to a seed-mediated growth method with slight modifications.[48] In brief, 4.7 mL of 0.1 M CTAB was mixed with 125 μL of 0.01 M $HAuCl_4 \cdot 3H_2O$ under vigorous stirring. Thereafter, ice-cold 30 μL of 0.1 M $NaBH_4$ was added to the mixture, and the color of the solution was immediately changed from yellow to brown under vigorous stirring, indicating the formation of the seed solution. The seed solution was continuously stirred for 2 h. To prepare Au NRs growth solution, 4.7 mL of 0.1 M of CTAB, 200 μL of 0.01 M $HAuCl_4 \cdot 3H_2O$, 30 μL of 0.01 M $AgNO_3$ and 32 μL of 0.1 M ascorbic acid were mixed in that order. Finally, 10 μL of seed solution was added the growth solution, and leaving this mixture overnight to ensure full growth of Au NRs.

2.4 Synthesis of AuNR@Ag nanostructure

AuNR@Ag nanostructure were prepared using slightly modified procedure that has been described previously.[49] 150, 250 and 350 μL of 0.01 M $AgNO_3$ were mixed with 4 mL of Au NRs separately, and then 20 μL of 0.1M Ascorbic acid and 250 μL of 0.1 M NaOH were sequentially added to increase the pH to 10. Within several minutes, the colors of these three solutions were changed, indicating the formation of AuNR@Ag. These mixtures were constantly stirred at 30 °C for 2 h.

2.5 AuNR@Ag based Sensor for Cr(VI) detection

1 mL of AuNR@Ag was placed in a 4 ml Vial, and a certain amount of 1 M HCl was added to the solution to decrease the pH to 3. Then Cr(VI) containing samples of various concentrations were added to the pH 3 AuNR@Ag colloid solutions. The resulting colloid solutions were stored at room temperature for 10 min. The extinction spectra of the colloid solution was recorded by UV-vis spectrometer. HR-TEM images were observed to characterize the morphology of AuNR@Ag after reacted with Cr(VI) containing samples of various concentrations.

3. Results and discussion

3.1 Characterization of AuNR@Ag with different Ag nanoshell thickness

UV-vis absorption spectroscopy was used to measure the as-prepared Au NRs. Due to the anisotropic morphology of the Au NRs, the dipole plasmon resonance is split into a transverse plasmon absorption at 532 nm and a longitudinal plasmon absorption at longer wavelength of 774 nm (Figure 5A). Typical TEM image (Figure 5B) of the as-prepared Au NRs revealed the average aspect ratio to be 3.5 (length and width of the Au NRs are 39.5 ± 3.8 nm and 11.4 ± 1.1 nm, respectively). In order to evaluate the effect of the Ag nanoshell thickness on the sensing performance, Au NRs with Ag nanoshells of different thickness were prepared according to the literature.[49] Figure 6 shows that the thickness of the Ag nanoshells could be tuned by using different amounts of silver nitrate. Compared to the UV-visible spectrum of Au NRs (Figure 5A), the longitudinal LSPR of the AuNR@Ag (Figure 6A) exhibited significant blue shifting and enhanced absorbance intensity. As shown in Figure 6A, with increasing Ag nanoshells thickness, the plasmon resonance peak of the AuNR@Ag was shifted from 590 nm to 573 nm and 535 nm, and the color of the AuNR@Ag solutions was

gradually changed from green to puple and red. Three SPR peaks could be observed and were designed as peaks 1-3 from long to short wavelength. Peak 3 implies that the plasmonic properties of silver are manifested and improved optical properties compared to gold .[50] As Au NRs were coated with silver, peak 1, which is longitudinal SPR peak blue-shifted, was accompanied with enhanced absorbance intensity. Peak 2, related to the transverse SPR peak, remains unchanged and the absorbance intensity of Peak 1-3 is gradually enhanced by increase the thickness of Ag nanoshell.[51] The core-shell nanostructure could be clearly observed in Figure 6B. As the amount of reduced silver increases, the shape of the particles approached an orange slice-like shape. The HR-TEM observation reveals that the deposited Ag nanoshells on Au NRs in the transverse direction were significantly thicker than in the longitudinal direction. The side facet of Ag nanoshells was varied from 4.6 nm to 6.9 nm and 10 nm by adjusting the amount of silver nitrate (Figure 6B). Further, the EDS analysis clearly showed that Au was in the core and Ag was in the shell (Figure 6C). There appeared to be good agreement with HR-TEM observations.

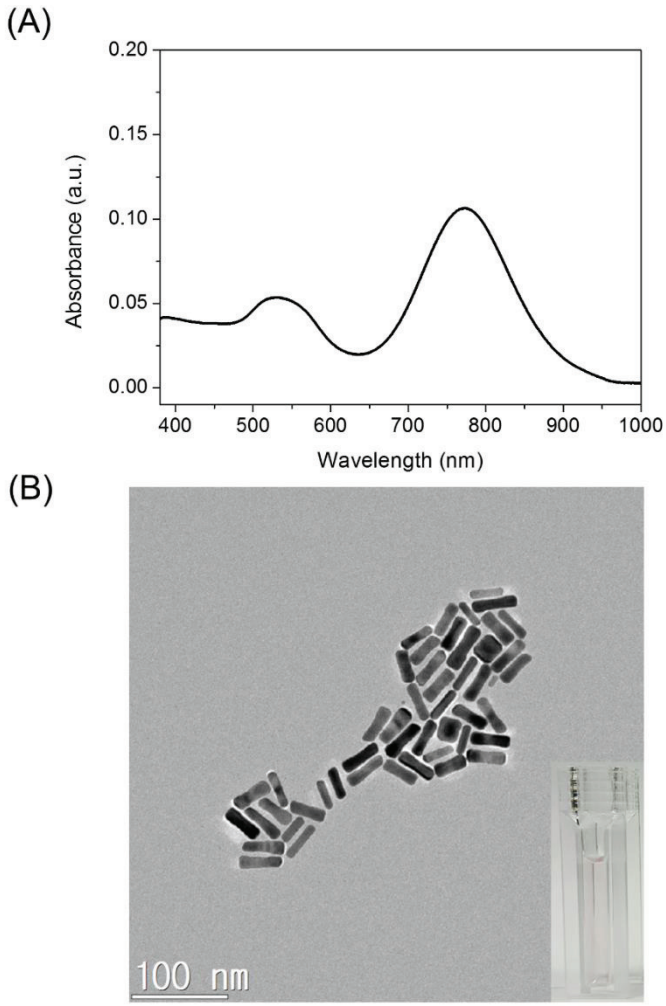

Figure 5 (A) UV-vis absorption spectrum of Au NRs. (B) TEM image of the Au NRs. (Inset: photograph of the Au NRs colloid solutions)

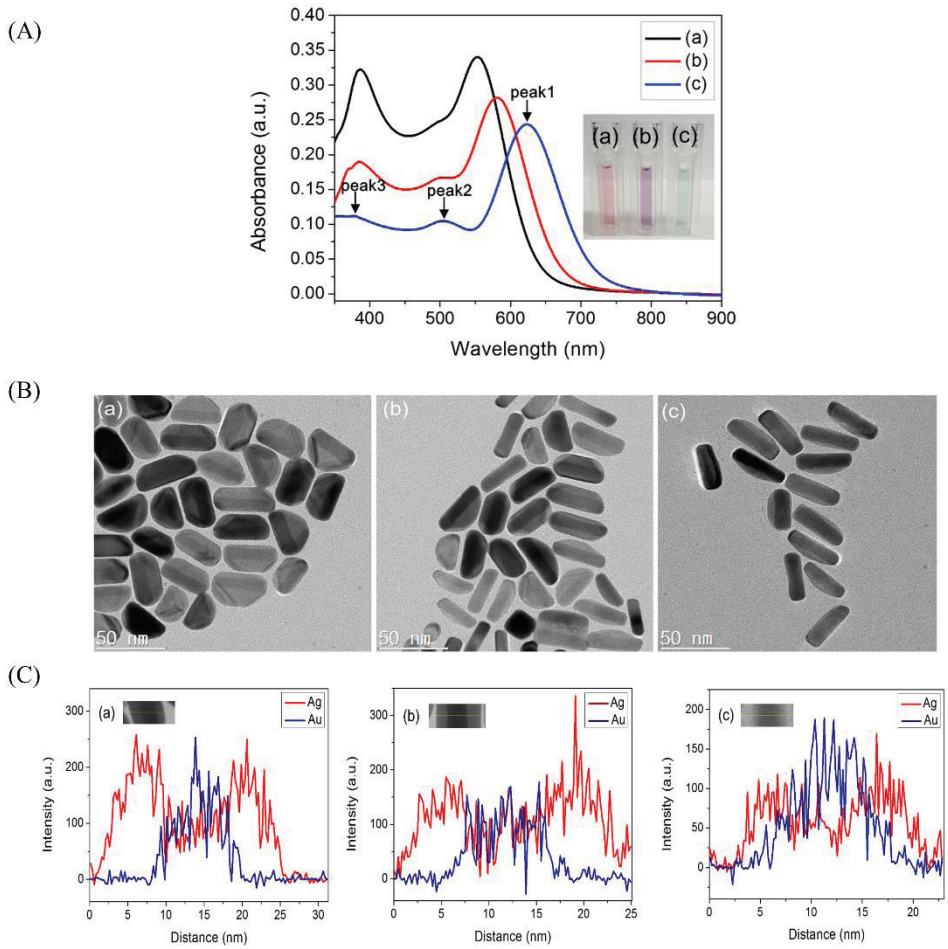

Figure 6 (A) UV-vis absorption spectra (Inset: photographs of the AuNR@Ag colloid with different Ag nanoshell thicknesses), (B) HR-TEM images and (C) EDX line-scanning profiles along the line in inset (C) of AuNR@Ag with different Ag nanoshell thickness obtained by changing the amounts of 0.01 M $AgNO_3$ to (a) 350 μL, (b) 250 μL, (c) 150 μL, respectively.

3.2 Sensing mechanism of Cr(VI) ions visual detection using AuNR@Ag nanostructures

In order to demonstrate the sensing mechanism of Cr(VI) ions visual detection using AuNR@Ag, the UV-vis spectra of the AuNR@Ag (obtained by coating 0.01 M $AgNO_3$ of 350 μL to Au NRs) as a function of reaction time after mixed with Cr(VI) ions was monitored (Figure 7A). Furthermore, the HR-TEM images demonstrated that the color change of the AuNR@Ag could be attributed to their morphological transition during the etching process (Figure 7B). The proposed etching mechanism for the detection of Cr(VI) was illustrated in Figure 8. A red-shift of the SPR wavelength was due to the decrease of the Ag nanoshell thickness, when the AuNR@Ag was reacted with Cr(VI) in aqueous solution. The etching of the Ag nanoshells could be explained by the theory of standard electrode potential between Ag and Cr(VI). The standard reduction potential of $Ag^+/Ag(s)$ and Cr(VI)/Cr(Ⅲ) are +0.7993 V and +1.36 V, respectively.[52] Accordingly, Cr(VI) ions could be reacted with Ag metal spontaneously to decrease the nanoshell thickness of the AuNR@Ag. When the concentration of Cr(VI) was increased, the Ag nanoshell thickness was decreased since more Ag metal was etched away. Accordingly, the significant morphological changes of AuNR@Ag with Cr(VI)

proved the viability of using this system to measure trace amounts of Cr(VI). To determine the sensitivity of the sensor, we recorded the UV-vis spectra of the AuNR@Ag in the presence of various concentrations of Cr(VI). Furthermore, we investigate the effect of the Ag nanoshell thickness of the AuNR@Ag on Cr(VI) detection. The AuNR@Ag with different Ag nanoshell thicknesses obtained by changing the amounts of 0.01 M $AgNO_3$ to 350 μL, 250 μL, and 150 μL, were prepared and called AuNR@Ag1, AuNR@Ag2, AuNR@Ag3, respectively. As the concentration of Cr(VI) increases, the absorbance intensity of AuNR@Ag1 was found to be decreased significantly and the color of the AuNR@Ag1 solution changed from red to purple, green and light violet, sequentially (Figure 9A). The absorbance displays a good linear response over the range from 10 to 60 μM and the detection limit was measured to be 600 nM. The absorbance intensity of AuNR@Ag2 was slightly lower than that of AuNR@Ag1 and the color of the solutions was changed gradually from purple to green and light-violet with the increase of Cr(VI) concentration (Figure 9B). The Cr(VI) detection system based on AuNR@Ag2 showed a linear response from 5 to 35 μM, with a detection limit as low as 300 nM. As seen from Figure 9C, the absorbance intensity of AuNR@Ag3 was lower than that of AuNR@Ag1 and Au@Ag-NR2. The linear response ranged from 2 μM to 12 μM and the limit of detection of Cr(VI) was 20

nM. In all experiments mentioned above, with an increase of Cr(VI) ion concentration, a progressive red-shift in the LSPR peak wavelength was observed due to the etching of Ag nanoshells and the LSPR of Au NRs caused by the complete etching of the Ag nanoshell. However, thin Ag nanoshells lead to a quicker red-shift, resulting in improved sensitivity but narrow linear range compared with thick Ag nanoshells. Thick Ag nanoshells expand the linear range but brings down the sensitivity (Figure 9A). As shown in Figure 9D, a linear relationship between the absorbance and Cr(VI) concentrations in the range of 2 μM to 60 μM was obtained. Among the three samples, we choose AuNR@Ag3, since it displayed the lowest detection limit. The sensing performance using AuNR@Ag3 was optimized with regard to the effect of CTAB and pH. Furthermore, the stability of the sensing method was studied over time intervals from 600 to 6000 s (Figure 10). The results showed that the sensing performance remain unchanged in 10-100 min, which demonstrated its good stability.

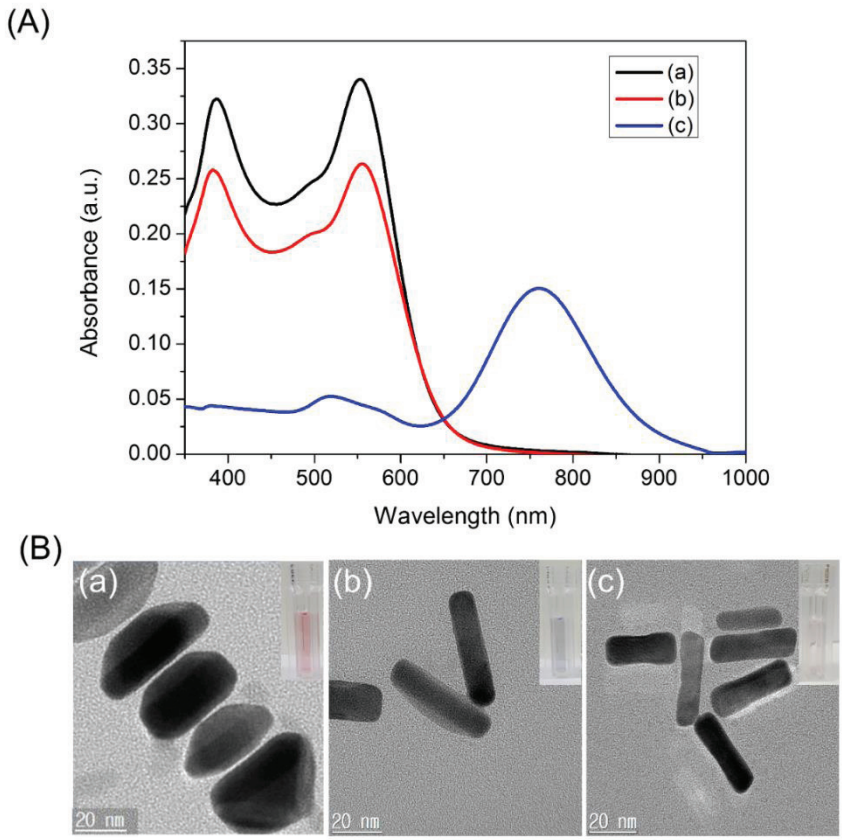

Figure 7 (A) UV-vis absorption spectra and (B) HR-TEM images of: (a) original AuNR@Ag(obtained by coating 0.01 M $AgNO_3$ of 350 μL to Au NRs), (b) AuNR@Ag after reacted with 10 μM of Cr(VI) and (c) AuNR@Ag after reacted with 60 μM of Cr(VI). (Insets: photographs of each AuNR@Ag colloid solutions)

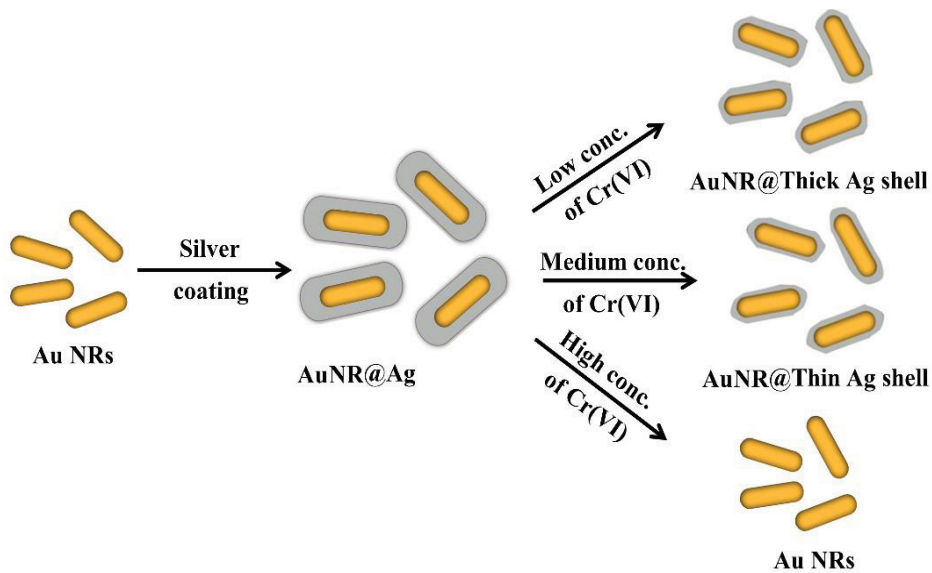

Figure 8 Schematic mechanism of sensing Cr(VI) based on etching of the AuNR@Ag nanostructures.

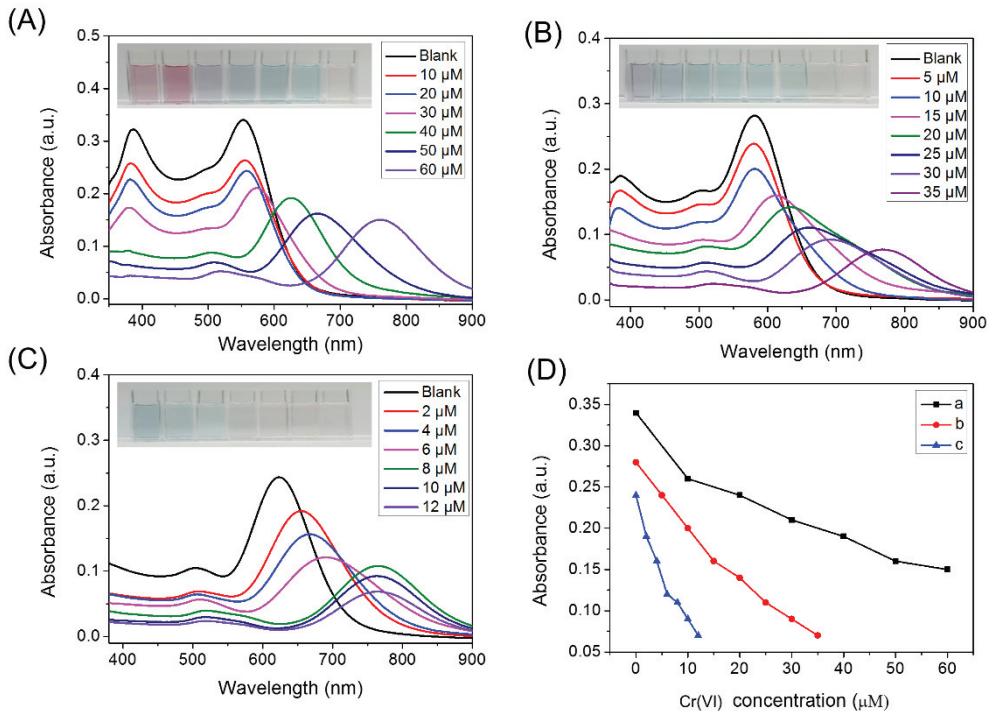

Figure 9 UV-vis absorption spectra of Au NRs coated with Ag nanoshell of different thicknesses resulting from adding the different amounts of silver nitrate. The absorption spectra of various concentrations of Cr(VI): (A) from 10 μM to 60 μM in AuNR@Ag1(Au NRs coated with 350 μL of 0.01 M $AgNO_3$), (B) from 5 μM to 35 μM in AuNR@Ag2 (Au NRs coated with 250 μL of 0.01 M $AgNO_3$), (C) from 2 μM to 12 μM in AuNR@Ag3(Au NRs coated with 150 μL of 0.01 M $AgNO_3$) (Insets: photograph of the color change AuNR@Ag colloids upon the addition of Cr(VI) with different concentrations). (D) Dose response curves for Cr(VI) detection with (a) AuNR@Ag1, (b) AuNR@Ag2 and (c) AuNR@Ag3.

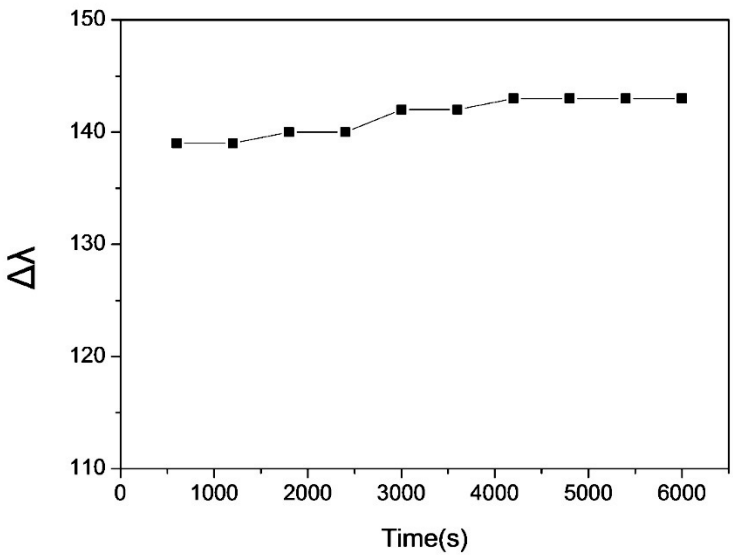

Figure 10 Effect of reaction time on the peak shift of the AuNR@Ag3 sensing system with adding 10 μM Cr(VI).

3.3 Optimization of the conditions for Cr(VI) measurement

In the pH range of 1-7, the wavelength shift of the AuNR@Ag shows different responses to Cr(VI). As shown in Figure 11A, the etching rate of the AuNR@Ag3 increases as the pH value decrease, which was ascribed to the increase of the electron potential and the increase of reduction ability of Cr(VI) as pH decreases. However, at lower pH, the AuNR@Ag3 becomes very unstable while at a pH higher than 3, the sensitivity deteriorates. Hence, pH 3 was considered to be the ideal working condition for this system. We also studied the effect of the concentration of CTAB, as shown in Figure 11B. The as-prepared AuNR@Ag3 was coated with CTAB molecules, which was positively charged. The large amount of CTAB coated on the surface of the AuNR@Ag3 would be interfere with chemical etching process. It was reported in literature that the positive charges induced by CTAB lowers sensitivity and selectivity of proposed sensing method.[53] Since the CTAB acts as a stabilizer to protect the AuNR@Ag3 against aggregation, the obtained AuNR@Ag3 with low concentration of CTAB was unstable. After careful study, the optimum concentration of CTAB was selected as 0.1 M.

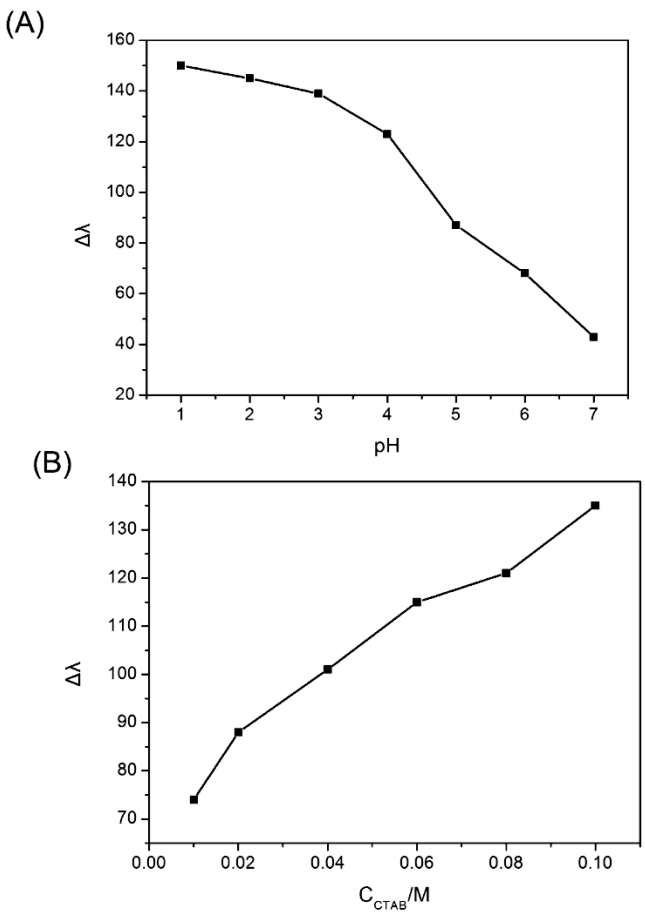

Figure 11 Effect of (A) pH and (B) concentration of CTAB on the peak shift (Δλ) of AuNR@Ag3 in the presence of 10 μM Cr(VI).

3.4 Selectivity of AuNR@Ag based sensor

To evaluate the selectivity of the AuNR@Ag3 based sensor towards Cr(VI) detection, 18 kinds of metal ions (Ag^{+}, Al^{3+}, Ba^{2+}, Ca^{2+}, Cd^{2+}, Co^{+}, Fe^{2+}, Hg^{2+}, K^{+}, Li^{+}, Mg^{2+}, Mn^{2+}, Na^{+}, Ni^{+}, Pb^{2+}, Zn^{2+}) were added to AuNR@Ag3 colloid solutions at the optimized conditions. The 18 kinds of metal ions were tested at a concentration of 100 μM, which was 100 times greater than that of Cr(VI). Figure 12 shows the photographic image and UV-vis spectra of the AuNR@Ag3 based detection systems with various metal ions. As shown in the photographic image (Figure 12A), only Cr(VI) ions caused obvious color change from green to light-violet. UV-vis spectrum of the AuNR@Ag3 based detection system showed a significant wavelength shift and decrease in the plasmonic intensity after the addition of 1 μM Cr(VI) (Figure 12B). In comparison with existing methods, the present method exhibited better analytical performance over other methods as summarized in Table 1.

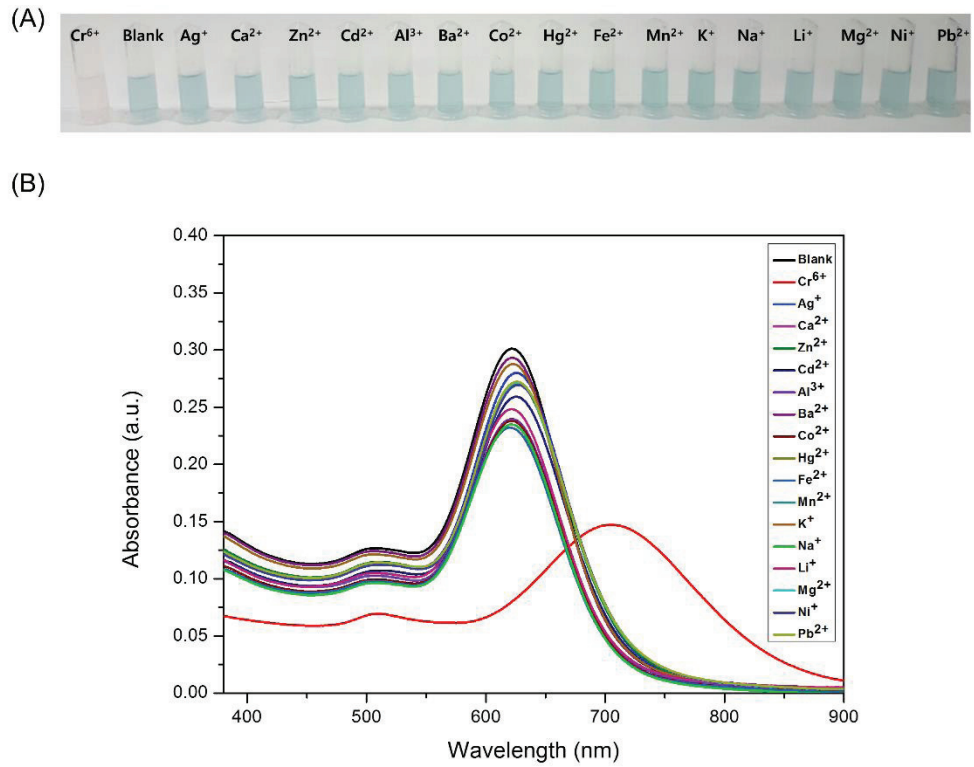

Figure 12 Selectivity of the AuNR@Ag3 sensing system. (A) Photographic images and (B) the UV-vis spectra of AuNR@Ag3 based detection systems with various metal ions. (The concentration of Ag^{+}, Ca^{2+}, Zn^{2+}, Cd^{2+}, Al^{3+}, Ba^{2+}, Co^{2+}, Hg^{2+}, Fe^{2+}, Mn^{2+}, K^{+}, Na^{+}, Li^{+}, Mg^{2+}, Ni^{+}, or Pb^{2+} was 1×10^{-4} M and the concentration of Cr(VI) was 1×10^{-6} M)

Table 1A comparison of the performance of different analytical methods for detection of Cr(VI).

Probe	Targets	Detection method	Time required for the assay (min)	LOD	Ref.
PTFE packed column	Cr(VI)	FAAS	—	0.8 μg/L	[54]
^{52}Cr and ^{53}Cr isotopes	Cr(III), Cr(VI)	ICP-MS	120	0.32 μM	[9]
AuNPs-ITO electrodes	Cr(VI)	Electrochemical	instant	2 μM	[55]
AuNPs-SPE	Cr(VI)	Electrochemical	instant	5 μg/L	[56]
Glutathione-CdTe quantum dots	Cr(VI)	Fluorescence	40	0.008 μg/mL	[57]
Graphene quantum dots	Cr(VI)	Fluorescence	2	3.7 nM	[58]
Fe_3O_4@Ag SERS substrate	Cr(VI)	SERS	instant	5 μg/L	[59]
BSA-Au NPs	Cr(VI)	Colorimetric	10	2.8 μM	[60]
DMSA-Au NPs	Cr(III), Cr(VI)	Colorimetric	5	10 nM	[42]
Ag NPs	Cr(VI)	Colorimetric	5	1 nM	[43]
Au NRs	Cr(VI)	Colorimetric	32	88 nM	[53]
Dumbbell-shaped Au NRs	Cr(VI)	Colorimetric	35	71 nM	[44]
AuNR@Ag	Cr(VI)	Colorimetric	10	20 nM	This work

3.5 Determination of Cr(VI) in real water samples

To evaluate the practical application of our proposed method for Cr(VI) detection, this assay was applied for the determination of trace Cr(VI) in real samples including tap water and lake water (from Gwanggyo, Gyeonggi-do, Korea**)**. Initially, the collected water samples were filtered two times through a membrane to remove any unwanted residue and added with standard Cr(VI) solution. Our proposed colorimetric method was compared with inductively coupled plasma-mass spectrometry (ICP-MS) method. The analytical results were listed in Table 2. The results obtained by both methods were in good agreement, indicating applicability of our designed colorimetric method for the detection of Cr(VI) in real water samples.

Table 2 Results for the determination of Cr(VI) ions in different environmental samples.

Samples	Added (μg L^{-1})	Found (μg L^{-1})[a]	Recovery (%)	Found by ICP-MS
Tap water	5	5.34 ± 0.1	93.6	5.13
Pond water	5	5.21 ± 0.2	96.0	5.09

[a] Mean standard deviation %.

4. Conclusions

In summary, a simple and cost-effective colorimetric method for the determination of trace Cr(VI) ions using AuNR@Ag as sensing probes is proposed. The sensing mechanism relies on the redox reaction between Cr(VI) ions and Ag nanoshells on Au NRs. As the concentration of Cr(VI) ions increased, more significant red-shift of the longitudinal peak and intensity decrease of the transverse peak could be observed. Several parameters such as concentration of CTAB, thickness of the Ag nanoshells and pH of the sample were carefully optimized to determine Cr(VI) ions. Under optimized condition, this method showed a low detection limit of 20 nM and high selectivity towards Cr(VI) over other metal ions, and the detection range of Cr(VI) could be tuned by controlling thickness of the Ag nanoshells. Real sample tests confirm the practicability of the method for environmental field analysis of trace Cr(VI) with good performance.

References

[1] D.M. Stearns, *BioFactors* 11(3) (2000) 149-162.

[2] W. Mertz, *J Nutr* 123(4) (1993) 626-633.

[3] W.H. Glinsmann, W. Mertz, *Metabolism* 15(6) (1966) 510-520.

[4] J. Martin, Z.Q. Wang, X.H. Zhang, D. Wachtel, J. Volaufova, D.E. Matthews, W.T. Cefalu, *Diabetes care* 29(8) (2006) 1826-1832.

[5] S. De Flora, M. Bagnasco, D. Serra, P. Zanacchi, *Mutat. Res* 238(2) (1990) 99-172.

[6] A. Zhitkovich, *Chem. Res. Toxicol.* 18(1) (2005) 3-11.

[7] M. Costa, *Toxicol. Appl. Pharmacol.* 188(1) (2003) 1-5.

[8] V. Gomez, M. Callao, *Trac-Trend Anal. Chem.* 25(10) (2006) 1006-1015.

[9] H. Gürleyük, D. Wallschläger, *J. Anal. Atom. Spectrom.* 16(9) (2001) 926-930.

[10] C. Williams, D.J. David, O. Iismaa, *J. Agr. Sci.* 59(03) (1962) 381-385.

[11] P. Liang, T. Shi, H. Lu, Z. Jiang, B. *Hu, Spectrochim. Acta Part B At. Spectrosc.* 58(9) (2003) 1709-1714.

[12] S. Xing, H. Xu, G. Shi, J. Chen, L. Zeng, L. Jin, *Electroanal.* 21(15) (2009) 1678-1684.

[13] N.J. Ronkainen, H.B. Halsall, W.R. Heineman, *Chem. Soc. Rev.* 39(5) (2010) 1747-1763.

[14] P.K. Jain, X. Huang, I.H. El-Sayed, M.A. El-Sayed, *Accounts Chem. Res.* 41(12) (2008) 1578-1586.

[15] C. McDonagh, C.S. Burke, B.D. MacCraith, *Chem. Rev.* 108(2) (2008) 400-422.

[16] A. El-Ansary, L.M. Faddah, *Nanotechnol. Sci. Appl.* 3(1) (2010) 65-76.

[17] H. Jans, Q. Huo, *Chem. Soc. Rev.* 41(7) (2012) 2849-2866.

[18] M. Li, H. Gou, I. Al-Ogaidi, N. Wu, *ACS Sustainable Chem. Eng.* 1(7) (2013) 713-723.

[19] S. Zeng, D. Baillargeat, H.-P. Ho, K.-T. Yong, *Chem. Soc. Rev.* 43(10) (2014) 3426-3452.

[20] M. Li, S.K. Cushing, N. Wu, *Analyst* 140(2) (2015) 386-406.

[21] B. Sepúlveda, P.C. Angelomé, L.M. Lechuga, L.M. Liz-Marzán, *Nano Today* 4(3) (2009) 244-251.

[22] J. Homola, *Chem. Rev.* 108(2) (2008) 462-493.

[23] N.E. Motl, A.F. Smith, C.J. DeSantis, S.E. Skrabalak, *Chem. Soc. Rev.* 43(11) (2014) 3823-3834.

[24] P.C. Ray, *Chem. Rev.* 110(9) (2010) 5332-5365.

[25] J. Pérez-Juste, I. Pastoriza-Santos, L.M. Liz-Marzán, P. Mulvaney, *Coord. Chem. Rev.* 249(17–18) (2005) 1870-1901.

[26] H. Chen, L. Shao, Q. Li, J. Wang, *Chem. Soc. Rev.* 42(7) (2013) 2679-2724.

[27] S. Link, M.B. Mohamed, M.A. El-Sayed, *J. Phys. Chem. B.* 103(16) (1999) 3073-3077.

[28] J.S. Lee, M.S. Han, C.A. Mirkin, Angew. Chem. Int. Ed. 46(22) (2007) 4093-4096.

[29] T. Lou, L. Chen, Z. Chen, Y. Wang, L. Chen, J. Li, *Appl. Mater. Interfaces* 3(11) (2011) 4215-4220.

[30] C. Radhakumary, K. Sreenivasan, *Anal. Chem.* 83(7) (2011) 2829-2833.

[31] L. Vigderman, B.P. Khanal, E.R. Zubarev, *Adv. Mater.* 24(36) (2012) 4811-4841.

[32] K. Saha, S.S. Agasti, C. Kim, X. Li, V.M. Rotello, *Chem. Rev.* 112(5) (2012) 2739-2779.

[33] J.-J. Feng, H. Guo, Y.-F. Li, Y.-H. Wang, W.-Y. Chen, A.-J. Wang, *Appl. Mater. Interfaces* 5(4) (2013) 1226-1231.

[34] S. Jayabal, A. Pandikumar, H.N. Lim, R. Ramaraj, T. Sun, N.M. Huang, *Analyst* 140(8) (2015) 2540-2555.

[35] K.A. Willets, R.P.V. Duyne, *Annu. Rev. Phys. Chem.* 58(1) (2007) 267-297.

[36] J. Cao, T. Sun, K.T.V. Grattan, *Sensors Actuat. B-Chem.* 195 (2014) 332-351.

[37] Z. Wang, L. Ma, Coord. *Chem. Rev.* 253(11) (2009) 1607-1618.

[38] D. Vilela, M.C. González, A. Escarpa, *Anal. Chim. Acta* 751 (2012) 24-43.

[39] Y. Zhou, S. Wang, K. Zhang, X. Jiang, *Angew. Chem.* 120(39) (2008) 7564-7566.

[40] N. Yang, Y. Gao, Y. Zhang, Z. Shen, A. Wu, *Talanta* 122 (2014) 272-277.

[41] W.Y. Xie, W.T. Huang, J.R. Zhang, H.Q. Luo, N.B. Li, *J. Mater. Chem.* 22(23) (2012) 11479-11482.

[42] W. Chen, F. Cao, W. Zheng, Y. Tian, Y. Xianyu, P. Xu, W. Zhang, Z. Wang, K. Deng, X. Jiang, *Nanoscale* 7(5) (2015) 2042-2049.

[43] A. Ravindran, M. Elavarasi, T. Prathna, A.M. Raichur, N. Chandrasekaran, A. Mukherjee, *Sensors Actuat. B-Chem.* 166 (2012) 365-371.

[44] S.A. Alex, J. Satija, M.A. Khan, G.M. Bhalerao, S. Chakravarty, B. Kasilingam, A. Sivakumar, N. Chandrasekaran, A. Mukherjee, *Anal. Methods* 7(13) (2015) 5583-5592.

[45] K. Park, R.A. Vaia, *Adv. Mater.* 20(20) (2008) 3882-3886.

[46] T.K. Sau, A.L. Rogach, F. Jäckel, T.A. Klar, J. Feldmann, *Adv. Mater.* 22(16) (2010) 1805-1825.

[47] F. Zhang, J. Zhu, J.-J. Li, J.-W. Zhao, *J. Mater. Chem. C* 3(23) (2015) 6035-6045.

[48] T.K. Sau, C.J. Murphy, *Langmuir* 20(15) (2004) 6414-6420.

[49] Y. Xiang, X. Wu, D. Liu, Z. Li, W. Chu, L. Feng, K. Zhang, W. Zhou, S. Xie, *Langmuir* 24(7) (2008) 3465-3470.

[50] R. Jiang, H. Chen, L. Shao, Q. Li, J. Wang, *Adv. Mater.* 24(35) (2012).

[51] T.Y. Olson, A.M. Schwartzberg, C.A. Orme, C.E. Talley, B. O'Connell, J.Z. Zhang, *J. Phys. Chem. C.* 112(16) (2008) 6319-6329.

[52] S.G. Bratsch, *J. Phys. Chem. Ref. Data* 18(1) (1989) 1-21.

[53] F.-M. Li, J.-M. Liu, X.-X. Wang, L.-P. Lin, W.-L. Cai, X. Lin, Y.-N. Zeng, Z.-M. Li, S.-Q. Lin, *Sensors Actuat. B-Chem.* 155(2) (2011) 817-822.

[54] A.N. Anthemidis, G.A. Zachariadis, J.-S. Kougoulis, J.A. Stratis, *Talanta* 57(1) (2002) 15-22.

[55] M.-C. Tsai, P.-Y. Chen, *Talanta* 76(3) (2008) 533-539.

[56] G. Liu, Y.-Y. Lin, H. Wu, Y. Lin, *Environ. Sci. Technol.* 41(23) (2007) 8129-8134.

[57] L. Zhang, C. Xu, B. Li, *Microchim. Acta* 166(1-2) (2009) 61-68.

[58] S. Huang, H. Qiu, F. Zhu, S. Lu, Q. Xiao, *Microchim. Acta* 182(9-10) (2015) 1723-1731.

[59] J. Du, C. Jing, *J. Colloid Interface Sci.* 358(1) (2011) 54-61.

[60] J.-f. Guo, D.-q. Huo, M. Yang, C.-j. Hou, J.-j. Li, H.-b. Fa, H.-b. Luo, P. Yang, *Talanta* 161 (2016) 819-825.

국 문 초 록

본 연구에서는 독성이 강한 6가 크로뮴 검출을 위해 간편하고, 저렴하며, 중금속 검출을 위해 별도의 장치가 불필요한 육안 식별 가능한 색 센서를 개발하였다. 이 색 센서는 은 나노 쉘을 코팅한 금 나노 막대를 이용한다. 높은 표면 플라즈몬 공명(Localized surface plasmon resonance) 특성을 갖는 금 나노 막대를 시드 매개 성장 법 (seed-mediated growth method)을 약간 변형하여 합성하였다. 이 후 합성한 금 나노 막대 입자에 은 나노 쉘을 코팅할 때 $AgNO_3$의 양을 조절하며 은 나노 쉘의 두께를 조절하였다. 금 나노 막대와 은 나노 쉘이 코팅된 금 나노 막대의 크기와 형태는 HR-TEM, EDS를 통해 분석하였으며, 광학적 특성은 UV-Vis spectrometer를 통해 분석하였다. 이 센서는 6가 크로뮴과 은 나노 쉘의 산화 환원과 관련된 메커니즘을 이용한다. 6가 크로뮴 농도에 따라 은 나노 쉘을 코팅한 금 나노 막대의 longitudinal peak 가 레드 쉬프트 되고 transverse peak의 intensity가 감소함으로써 이 센서가 6가 크로뮴에 반응 하는 것을 확인하였다. CTAB의 농도, pH, 은 나노 쉘의 두께를 최적화 하였다. 이

렇게 최적화한 상태에서 이 색 센서는 낮은 측정 한계치(20 nM)를 나타내었으며 높은 선택성을 가지고 있다. 또한 은 나노 쉘의 두께조절을 통해 검출 범위를 조절할 수 있다. 실제 샘플 평가를 통해서도 확인 할 수 있듯이 이 색 센서는 대상 물질에 대한 즉각적인 정보를 제공하여, 실시간 현장 분석이 가능하게 해주며 선택성, 민감도가 뛰어나다. 이를 통해, 6가 크로뮴 검출 환경 색 센서로서 가능성을 볼 수 있었다.

주요어 : 금 나노 막대, 은 나노 쉘, 6가 크로뮴 이온, 에칭, 색 센서

학 번 : 2015-26023